Supporting Information

Magnetic wire active microrheology of human respiratory mucus

Milad Radiom, Romain Hénault, Salma Mani, Aline Grein-Iankovski, Xavier Norel, Jean-François Berret*

Outline

SI 1 – Human mucus samples used in this study
SI 2 – Origin of the human mucus samples
SI 3 – Synthesis of magnetic wires
SI 4 – Characterization of magnetic wires
SI 5 – Effect of pH on the magnetic wire stability
SI 6 – Magnetic rotational spectroscopy: methods
SI 7 – Magnetic rotational spectroscopy *versus* macrorheology: a comparative study
SI 8 – Analysis of early *Ex Vivo* mucus
SI 9 – Review of previous sputum and mucus rheology data

Movie#1 – Wire rotation associated with Fig. 1a
Movie showing a 23 µm wire undergoing rotation in *Ex Vivo* mucus as a result of a 10 mT external magnetic field rotating with an angular frequency of 0.0094 rad s^{-1}.
Movie#2 – Wire rotation associated with Fig. 1b
Same as movie#1 for an angular frequency of 0.94 rad s^{-1}.
Movie#3 – Wire rotation associated with Fig. 4a
Movie showing a 23 µm wire undergoing rotation in Ex Vivo mucus as a result of a 10 mT external magnetic field rotating with an angular frequency of 0.0031 rad s^{-1}.
Movie#4 – Wire rotation associated with Fig. 4b
Same as Movie#3 at 0.0094 rad s^{-1}.

Revised version Friday, July 23, 2021 - Submitted to Soft Matter
Corresponding author*: jean-francois.berret@u-paris.fr

Supporting Information S1

Human mucus samples used in this study

Sample	Collection	Conditioning
Early *Ex Vivo*	Directly from bronchus tube	Room temperature, washed in Tyrode solution
Late *Ex Vivo*	From *Ex Vivo* culture of excised bronchus tube	12 – 18 h incubation (37°C, 5% CO_2)

Table S1*: Definitions of mucus samples.*

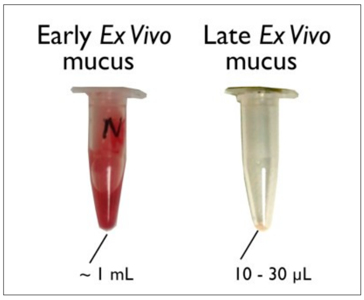

Figure S1*: Images of Eppendorf containing the early and late Ex Vivo mucus*

Supporting Information S2
Origin of the human mucus samples

Date of surgery	Sex	Age	Pulmonary diseases	Samples
23/01/2019	M	61	Pulmonary adenocarcinoma	Late *Ex Vivo* Early *Ex Vivo*
28/01/2019	M	58	Pulmonary hypertension and fibrosis	Late *Ex Vivo* Early *Ex Vivo*
21/03/2019	F	56	Pulmonary fibrosis	Late *Ex Vivo* Early *Ex Vivo*
16/04/2019	M	66	Pulmonary fibrosis	Late *Ex Vivo* Early *Ex Vivo*
21/05/2019*	M	n.s.	none	Early *Ex Vivo*
21/05/2019	M	56	Pulmonary fibrosis	Early *Ex Vivo*
06/06/2019	M	48	Pulmonary hypertension and fibrosis	Late *Ex Vivo*
04/07/2019	M	62	Pulmonary hypertension and fibrosis	Late *Ex Vivo* Early *Ex Vivo*

Table S2*: Patients pathologies. This patient designated with a star* was a donor with no identified respiratory disease. n.s. is for “not specified”.*

Supporting Information S3
Synthesis of magnetic microwires

Superparamagnetic maghemite (γ-Fe_2O_3) nanoparticles with a mean diameter of 13.2 nm and a dispersity of 0.23 are used (**Fig. S3-1**). The nanoparticles are initially coated with poly(acrylic) acid polymer at pH 2.0. The precipitate is then re-dispersed by increasing the pH to 10. The negatively charged particles are then assembled using poly(diallydimethyl ammonium chloride) (PDADMAC) polycations. The cylindrical shape was given during desalting the mixed solutions using a dialysis cassette under a magnetic field of 300 mT (**Fig. S3-2**).

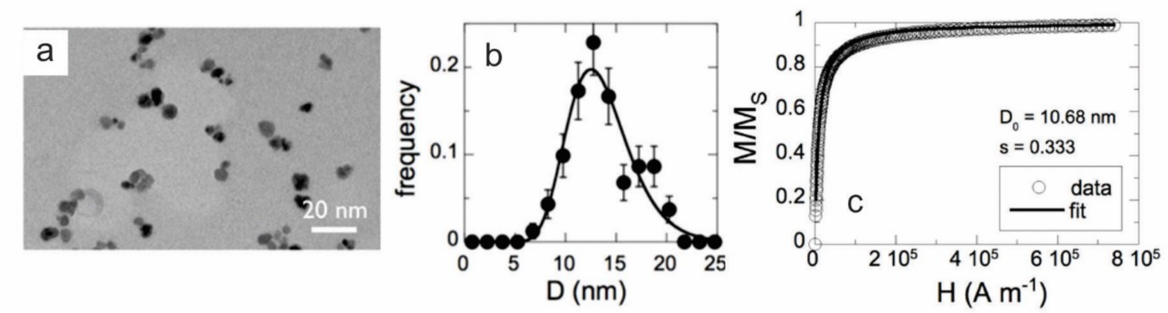

Figure S3-1*: (a-c) Iron oxide nanoparticles: transmission electron microscopy image (a), size distribution (b), and magnetic field H-dependence of the macroscopic magnetization M(H) normalized by its saturation value M_S for cationic (uncoated) maghemite dispersions (c). The experiment was performed using vibrating sample magnetometry (VSM). The solid curve was obtained using the Langevin equation convoluted with a log-normal distribution of particle sizes. $M_S = \phi \times m_s$, where m_s is the specific magnetization of colloidal maghemite ($m_s = 3.5\times10^5$ A m^{-1}) and ϕ the volume fraction. The nanoparticle diameter derived from VSM and from TEM are different, D_{TEM} = 13.2 nm versus D_{VSM} = 10.7 nm [1,2].*

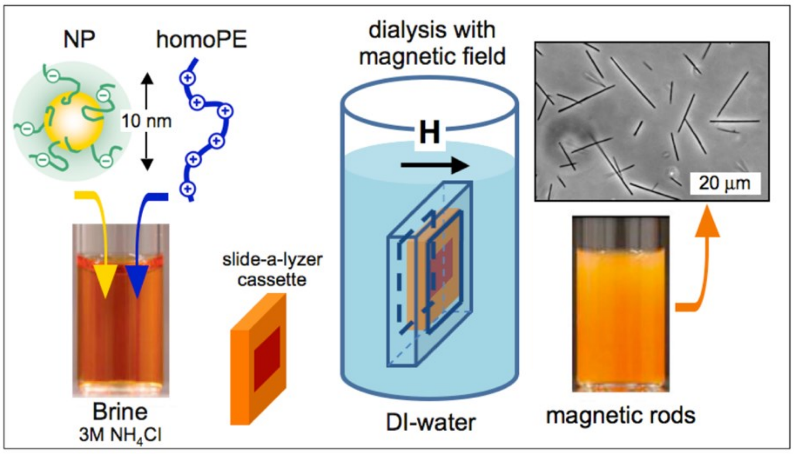

Figure S3-2*: Schematic representation of the protocol that controls the nanoparticle co-assembly and wire formation. The dialysis involves the preparation of separate 1 M NH_4Cl salted solutions of particles and oppositely charged polymers. The ionic strength is progressively diminished by dialysis with a 10000 g mol^{-1} cut-off Slide-a-Lyzer cassette. Light microscopy image of the wires is shown.*

Supporting Information S4

Characterization of magnetic microwires

The geometrical characterization of the microwires was performed by measuring the length (*L*) and the diameter (*D*) of wires using a 100× objective lens on an optical microscope (Olympus IX73) coupled with a CCD camera (QImaging, EXi Blue) supported by the software Metaview (Universal Imaging). **Fig. S4-1a**) displays the variation of the diameter as a function of the wire length, leading to $D(L) = 0.670L^{0.198}$. From this expression, we calculate the reduced wire length, $L^* = L/[D\sqrt{g(L/D)}]$, where $g(x) = ln(x) - 0.662 + 0.917x - 0.050x^2$ (**Fig. S4-1b**).

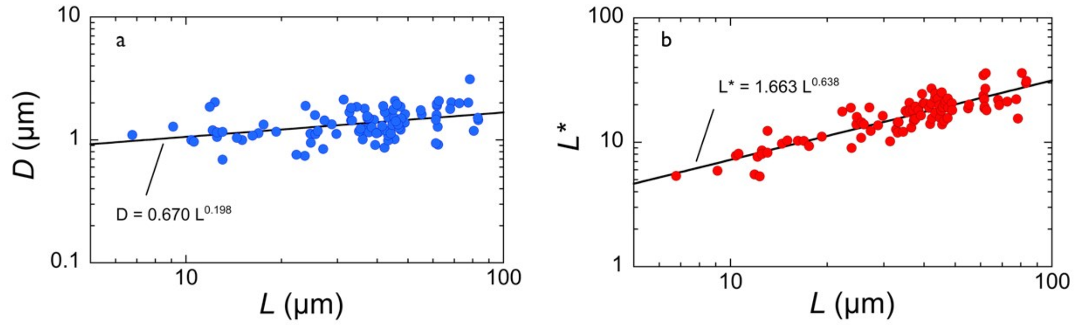

Figure S4-1: *Dependence of the diameter (D) and reduced wire length (L^*) as a function of the wire length (L). The straight lines are scaling laws with exponents 0.198 and 0.638 respectively.*

The anisotropy ratio ($\Delta\chi$) of the wires was calculated in independent measurements in fluids of known viscosity, such as water-glycerol mixtures. In this case, by collecting the critical frequency ω_C for wires of various reduced length L^*, $\Delta\chi$ was calculated using Eq. 2 in the main text. For these wires $\Delta\chi$ was found to be equal to 2.3 (**Fig. S4-2**).

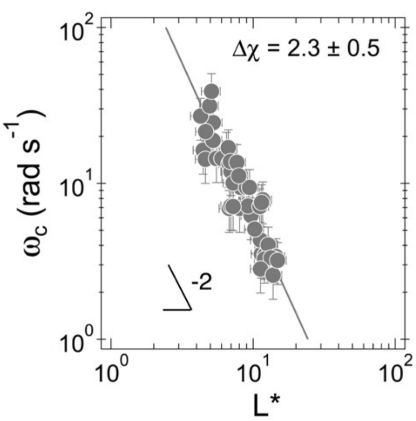

Figure S4-2: *Distribution of the critical frequency (ω_C) as a function of the reduced wire length (L^*) for wires in 85% glycerol-water solution of viscosity 0.062 Pa s^{-1} (T = 26 °C). The distribution is fit to Eq. 1 in the main text giving anisotropy ratio $\Delta\chi$ = 2.3 ± 0.5 [3].*

Supporting Information S5

Effect of pH on the magnetic wire stability

There are indications that airway defenses are affected by the pH of the lung fluids [4]. The pH of the airway mucosa has been measured and depending on the pathology the pH was found to vary between 5.5 and 8.3. In this context of microrheology measurements using magnetic wires, it is important to assess the stability of magnetic wires as a function of the pH. The pH of a dispersion containing 15 µm long wires (median value) was modified by addition of hydrochloric acid (pH 1.5, 3.4, 4.1) or sodium hydroxide (pH 9.1). After 4 days, the wires were observed by phase-contrast microscopy and compared to the neutral pH conditions [5-7]. **Fig. S5** shows that from pH 9.1 down to pH 3.4 the wires remained intact, and comparable to those of neutral conditions (pH 7.5). At pH 1.4, the wires changed slightly but were still not degraded. Few wires exhibit kinks and bending that indicate a softening of their structure.

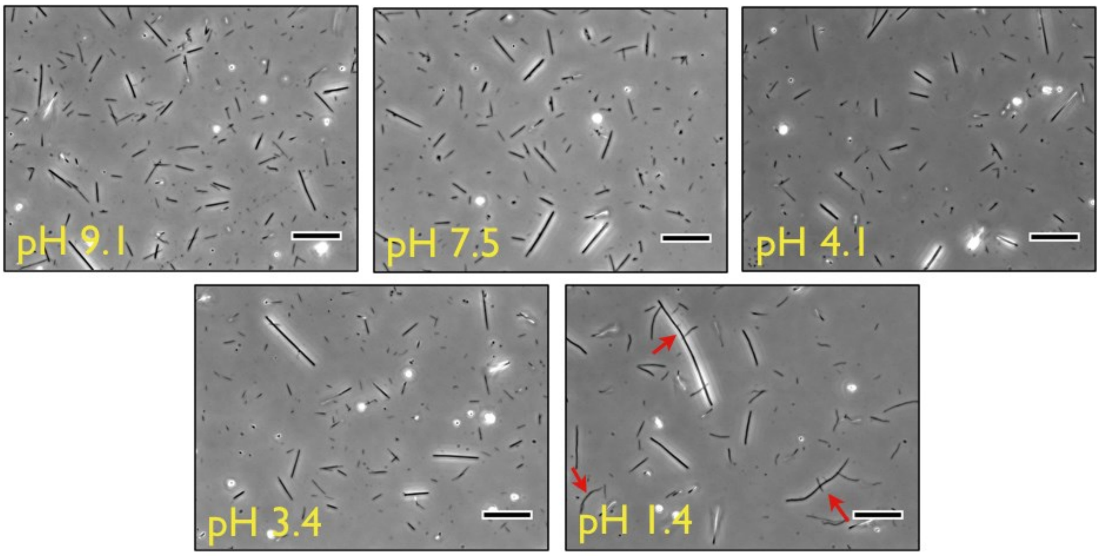

***Figure S5**: Phase-contrast images of magnetic wires at different pHs between pH 9.1 and pH 1.4.*

Supporting Information S6

Magnetic rotational spectroscopy methods

The magnetic device consists of two pairs of coils each 23 Ω. The current input to the coils is by a two-channel frequency generator and an amplifier. Using this setup which is schematically shown in **Fig. S6**, we applied rotating magnetic fields with an amplitude of 10.3 mT and a rotational velocity ranging from 0.001 – 10 rad s^{-1} to the wires in mucus. The evolution of wire orientation angles was acquired on IX73 Olympus inverted microscope with 20× objective lens and further analyzed using plug-ins in ImageJ.

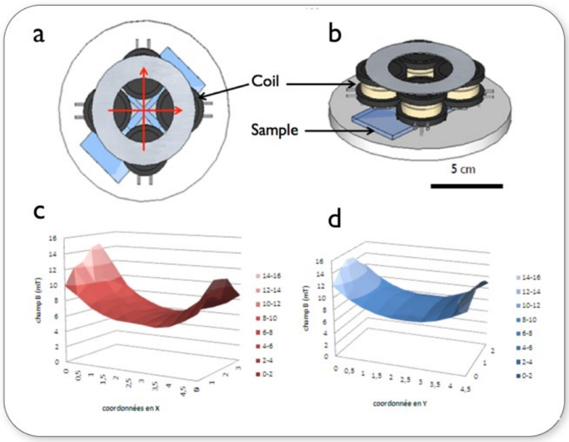

***Figure S6**: Top (a) and side (b) views of the rotating field device used in this work. Magnetic field distributions are shown along the X (c) and Y (d) axis of the four-coil device. In the center, the magnetic field is constant over a 1 × 1 mm^2 range.*

Supporting Information S7

Magnetic rotational spectroscopy *versus* macrorheology: a comparative study

Microrheology with a viscoelastic liquid model

A mixture of cetylpyridinium chloride (CPCl) and sodium salicylate (NaSal) dispersed in 0.5 M NaCl solution at a concentration of 2 wt.% forms a perfect (Maxwell) viscoelastic liquid. CPCl and NaSal are known to self-assemble spontaneously into micrometer long wormlike micelles, which then build a semi-dilute entangled network with a mesh size of 30 nm at the used concentration [8,9]. **Fig. S7-2a** displays a cone-and-plate device (diameter 50 mm, angle of the cone 2°, CSL 100 rheometer, TA Instruments) used in macrorheology and **Fig. S7-2b** the frequency dependence of the elastic and viscous moduli $G^{'}(\omega)$ and $G^{''}(\omega)$ obtained with this solution. At 27 °C, the solution was characterized by a static viscosity $\eta_0 = 1.0 \pm 0.1$ Pa s, and an elastic modulus $G_0 = 7.1 \pm 0.1$ Pa [8]. The relaxation time of the solution is then estimated to be $\tau_R = 0.14$ s. The continuous lines are the predictions for a Maxwell fluid: $G^{'}(\omega)/G_0 = X^2/(1+X^2)$ and $G^{''}(\omega)/G_0 = X/(1+X^2)$ with $X = \omega\tau_R$. The agreement between the data and Maxwell model predictions is excellent. In **Fig. S7-2c and S7-2d**, a rotating magnetic field of 10.4 mT was applied to 8.1 µm wire (inset) immersed in the solution at increasing frequencies 0.1 – 20 rad s^{-1}. The motion of the wire was monitored by optical microscopy, and the time dependence of orientation angle derived. **Fig. S7-2c** show 4 experimental time traces $\theta(t)$ obtained at excitation frequencies 0.14, 0.40, 2.9 and 17.0 rad s^{-1}. At low frequency, the wire rotates with the field, and $\theta(t) = \omega t$. Above the critical frequency (here $\omega_c = 0.38$ rad s^{-1}), the wire performs turn-and-return response behavior characteristic of the asynchronous regime. The red straight lines in the figures represent the average angular velocity $\Omega(\omega)$. **Fig. S7-2d** displays the evolution of the average rotational velocity versus excitation frequency obtained with several wires investigated in this fluid. The data were adjusted using equation (1) and (2) in the main text and a value of the viscosity equal to 1.3 ± 0.3 Pa s, in good agreement with cone-and-plate rotational rheometry is obtained. The comparison between macro- and microrheology shows that rotating wires are able to account for the static shear viscosity of a Maxwell fluid.

Microrheology with a viscoelastic solid model

Phytagel powder was added slowly to 1 mM calcium chloride solution at room temperature with rapid stirring and heated up to 50°C. A final concentration equal to 0.3 wt.% was prepared higher than the sol to gel transition concentration. The sample was studied by cone-and-plate rheometry in the same conditions as the surfactant micelles. **Fig. S7-3a** displays the cone-and-plate geometry used for the rheological measurements and **Fig. S7-3b** the frequency dependences of the elastic and viscous moduli. We find that $G^{'}(\omega)$ and $G^{''}(\omega)$ exhibit scaling behaviors with exponents 0.20 and 0.15, respectively. In addition, on the whole frequency range, the inequality $G^{'}(\omega) > G^{''}(\omega)$ is found. These two properties are known to be indicators of a viscoelastic solid behavior [10,11]. In microrheology using MRS, wires of lengths 6 – 45 µm were immersed in the sample and submitted to a rotating magnetic field of 12 mT at a frequency between 5×10^{-3} – 10 rad s^{-1}. **Fig. S7-3c** shows time traces of the orientation angle obtained at 0.015, 0.15, 1.54 and 6.83 rad s^{-1}. Over 3 decades in frequency, the traces reveal a unique behavior: $\theta(t)$ displays regular oscillations at a frequency double of that of the field, and an average rotational velocity $\Omega(\omega)$ (shown as red straight lines). **Fig. S7-3d** displays the average rotational velocity *vs* the excitation frequency, and indicates that for all frequencies tested, $\Omega(\omega)\cong 0$ within the measurement uncertainty. This behavior agrees with the prediction for the Kelvin-Voigt model. From the amplitude of the oscillation $\theta_B(\omega)$, the elastic modulus $G = 2.5 \pm 2.8$ Pa is estimated using the expression of equation (3) in the main text in good agreement with the rheological cone-and-plate value $G^{'} = 3.0 \pm 0.5$ Pa. In conclusion, we show that our MRS technique is able to account for the time and frequency dependencies of a viscoelastic solid of Kelvin-Voigt type.

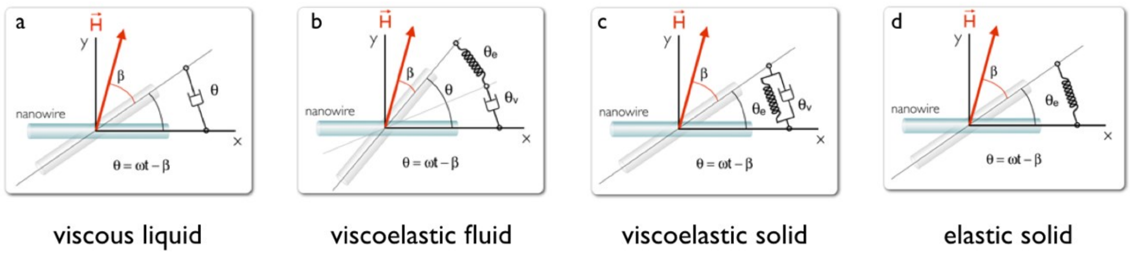

***Figure S7-1**: Schematic representation of a wire in a purely viscous liquid (a), viscoelastic liquid (b), viscoelastic solid (c) and elastic solid (d). The viscous liquid is shown as a dashpot and the elastic solid as a spring. A spring and a dashpot in series form a Maxwell element. A spring and a dashpot in parallel form a Kelvin-Voigt element.*

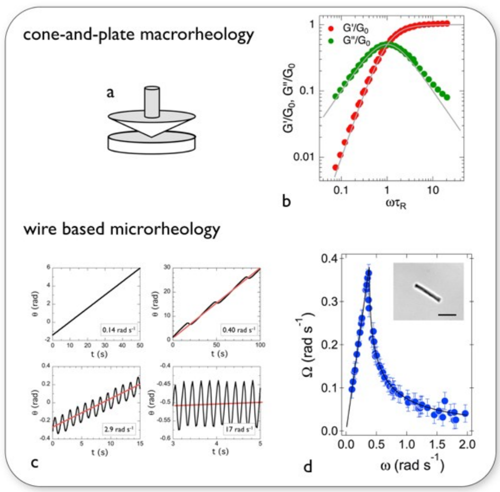

***Figure S7-2**: (a) Cone-and-plate geometry used in shear rheometry. (b) $G^{'}(\omega)/G_0$ and $G^{''}(\omega)/G_0$ vs frequency for a wormlike micellar fluid. The continuous lines are Maxwell predictions. (c) Orientation angle $\theta(t)$ of 8.1 µm wire as a function of the time and at several actuation frequencies 0.14, 0.40, 2.9 and 17.0 rad s^{-1}. (d) Average rotational velocity $\Omega(\omega)$ as a function of the frequency. The solid line corresponds to the best fit using equation (1) in the main text. Inset in (d): image of the wire by phase contrast microscopy (60×, scale bar 5 µm).*

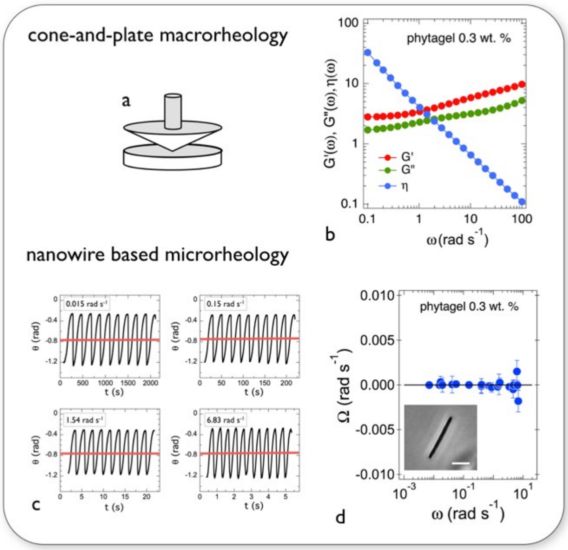

Figure S7-3*: (a) Cone-and-plate geometry used in shear rheometry. (b) $G^{'}(\omega)$, $G^{''}(\omega)$ and $\eta(\omega)$ vs frequency of a 0.3 wt.% phytagel sample. (c) Orientation angle $\theta(t)$ of 12 µm wire as a function of the time for various values of actuation frequency 0.015, 0.15, 1.54 and 6.83 rad s^{-1}. (d) Average rotational velocity $\Omega(\omega)$ as a function of the actuation frequency. The solid line corresponds to the best fit using the Kelvin-Voigt model. Inset in d): image of the 12 µm wire by phase contrast microscopy (60×, scale bar 5 µm).*

Supporting Information S8

Analysis of early *Ex Vivo* mucus

Early *Ex Vivo* mucus gels were studied using MRS following the protocol described in the main text. The proportions of the two generic behaviors (viscoelastic liquid and soft solid) were 35 cases to 23 cases in a total 58 wires investigated in 8 different samples. The data for the 35 wires in the viscoelastic liquid regime are described in details in the main text in Section 3.4. The angle θ_{eq} for 23 individual wires with soft solid response are plotted in Fig. S8 as a function of the reduced wire length. Using Eq. 3 (solid line in green), we calculated the equilibrium elastic modulus and obtained a mean of G_{eq} = 2.0 ± 0.2 Pa for the early *Ex Vivo* mucus.

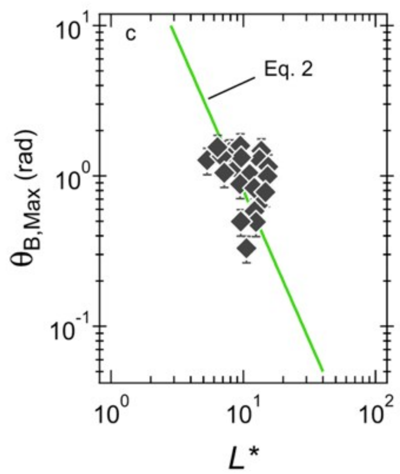

Figure S8: *Variation of oscillation amplitude* $\lim_{\omega\to 0} \theta_B(\omega)$ *as a function of the reduced wire length. Solid line shows the* $1/{L^*}^2$*-dependence of Eq. 3, leading to* G_{eq} = 2.0 ± 0.2 *Pa.*

Supporting Information S9

Review of previous sputum and mucus rheology data

Macro and microrheological data from the literature were evaluated for sputum and mucus from different human and animal sources and from related diseases, such as chronic obstructive pulmonary disease (COPD) and cystic fibrosis (CF).

		Mucus			Sputum			
	References	**Healthy**	**COPD**	**CF**	**Healthy**	**COPD**	**CF**	**Cells**
1	Dulfano-71 [12]					human		
2	King-81 [13]						canine	
3	Puchelle-81 [14]						human	
4	Jeanneret-Grosjean-88 [15]	human						
5	Shah-96 [16]						human	
6	Griese-97						human	
7	Sanders-00 [17]						human	
8	Dawson-03 [18]						human	
9	Besseris-07[19]	canine						
10	Suk-09 [20]						human	
11	Seagrave-12 [21]							human
12	Kirch-12 [22]	horse						
13	Schuster-13 [23]	human						
14	Tomaiuolo-14 [24]						human	
15	Vasquez-14 [25]	horse						
16	Hill-14 [26]					human	human	
17	Yuan-15 [27]				human		human	
18	Murgia-16 [28]	porcine						
19	Requena-17 [29]	human		human				
20	Ma-18 [30]						human	
21	Radtke-18 [31]						human	
22	Jory-19 [32]	human	human					
23	Patarin-20 [33]				human	human	human	

Table S9-1: *List of publications on the rheology of sputum and mucus. The references are arranged chronologically. In the first column, they are labeled with the name of the first author and the year of publication. The origin of the sputum and mucus samples studied is indicated.*

SPUTUM ELASTICITY DATA RELATED CYSTIC FIBROSIS

	References	**Nature**	ω **rad s^{-1}**	G' **(Pa)**	G'' **(Pa)**	G^* **(Pa)**	G' **(Pa) extrapolated at 1 rad s^{-1}**	G'' **(Pa) extrapolated at 1 rad s^{-1}**	G^* **(Pa) extrapolated at 1 rad s-1**
1	Puchelle-81 [14]	Human (CF)		1.5			1.5		
2	Shah-96 [16]	Human (CF)	100	34.3	13	46.8	17.2	13	23.4
3	Griese-97 [34]	Human (CF)	1			25			25.0
4	Griese-97 [34]	Human (CF)	100			63			31.5
5	Dawson-03 [18]	Human (CF)	1	6.0	2.5	6.5	1	6.0	2.5
6	Serisier-09 [35]	Human (CF)	56	2.25		7.8	1.2		4.3
7	Tomaiuolo-14 [24]	Human (CF)	1.0	1.0	0.3	1.05	1.0	0.3	1.05
8	Hill-14 [26]	Human (CF)	6.3	3.5	1.0	3.6	2.6	0.75	2.7
9	Yuan-15 [27]	Human (CF)	6.3	6.0	1.8	6.3	4.5	1.4	4.7
10	Patarin-20 [33]	Human (CF)	3.8	3.5	1.0		1.02	0.34	1.08
						n	**8**	**6**	**9**
						Average ± SE	**4.4 ± 1.9**	**3.0 ± 2.0**	**11.1 ± 4.0**

Table S9-2: *Storage, loss and complex elastic moduli G', G'' and G^* respectively obtained from literature data on cystic fibrosis sputum. The references are arranged chronologically. In the first column, they are labeled with the name of the first author and with the year of publication. In columns 4, 5, and 6 are indicated the moduli measured at angular frequencies provided in column 3. To facilitate comparison between different data, values obtained at frequencies other than ω = 1 rad s^{-1} were extrapolated to this angular frequency using the scaling laws found by Schuster et al. [23] on healthy human mucus, $G'(\omega) \sim \omega^{0.15}$ and $G''(\omega) \sim \omega^{0.15}$ (results average on n = 5 samples). Identical expressions were applied to sputum and mucus.*

HUMAN MUCUS ELASTICITY DATA

	References	**Nature**	ω **rad s^{-1}**	G' **(Pa)**	G'' **(Pa)**	G^* **(Pa)**	G' **(Pa) Extrapolated at 1 rad s^{-1}**	G'' **(Pa) extrapolated at 1 rad s^{-1}**	G^* **(Pa) Extrapolated at 1 rad s^{-1}**
1	Jeanneret-88 [15]	Human	1			14.1			14.1
2	Jeanneret-88 [15]	Human	100			33.9			17.0
3	Seagrave-12 [21]	Human	6.3	2.5	1	2.7	1.9	0.8	2.0
4	Schuster-13 [23]	Human	1	12	3.2	12.4	12.0	3.2	12.4
5	Jory-19 [32]	Human	1	7.9	2.2	8.2	7.9	2.2	8.2
						n	**3**	**3**	**5**
						Average ± SE	**7.3 ± 2.9**	**2.1 ± 0.7**	**10.7 ± 2.6**

Table S9-3: *Storage, loss and complex elastic moduli G', G'' and G^* respectively obtained from literature on human mucus samples. The extrapolation of the moduli to ω = 1 rad s^{-1} was performed as explained in Tab. S9-2.*

SPUTUM VISCOSITY DATA

	References	**Nature**	**Sputum viscosity (Pa s)**
1	Dulfano-71 [12]	Human (COPD)	200
2	Puchelle-81 [14]	Human (CF)	24.8
3	Dawson-03 [18]	human (CF)	50
4	Tomauiolo-14 [24]	human (CF)	10
5	Tomauiolo-14 [24]	human (CF)	50
		n	**5**
		Average ± SE	**67 ± 34**

Table S9-4: *Viscosity obtained from literature on human sputum samples.*

References

[1] J.-F. Berret, A. Sehgal, M. Morvan, O. Sandre, A. Vacher, M. Airiau, Stable oxide nanoparticle clusters obtained by complexation, *J. Colloid Interface Sci.*, 303 (**2006**) 315-318.
[2] J. Fresnais, M. Yan, J. Courtois, T. Bostelmann, A. Bee, J.F. Berret, Poly(acrylic acid)-coated iron oxide nanoparticles: Quantitative evaluation of the coating properties and applications for the removal of a pollutant dye, *J. Colloid Interface Sci.*, 395 (**2013**) 24-30.
[3] J.-F. Berret, Local Viscoelasticity of Living Cells Measured by Rotational Magnetic Spectroscopy, *Nat. Commun.*, 7 (**2016**) 10134.
[4] H. Fischer, J.H. Widdicombe, Mechanisms of Acid and Base Secretion by the Airway Epithelium, *The Journal of Membrane Biology*, 211 (**2006**) 139-150.
[5] J. Fresnais, J.-F. Berret, B. Frka-Petesic, O. Sandre, R. Perzynski, Electrostatic Co-Assembly of Iron Oxide Nanoparticles and Polymers: Towards the Generation of Highly Persistent Superparamagnetic Nanorods, *Adv. Mater.*, 20 (**2008**) 3877-3881.
[6] M. Yan, J. Fresnais, J.-F. Berret, Growth mechanism of nanostructured superparamagnetic rods obtained by electrostatic co-assembly, *Soft Matter*, 6 (**2010**) 1997-2005.
[7] M. Yan, J. Fresnais, S. Sekar, J.P. Chapel, J.-F. Berret, Magnetic Nanowires Generated via the Waterborne Desalting Transition Pathway, *ACS Appl. Mater. Interfaces*, 3 (**2011**) 1049-1054.
[8] J.-F. Berret, Rheology of wormlike micelles: Equilibrium properties and shear banding transitions, *Mol. Gels*, (**2006**) 667-716.
[9] S. Lerouge, J.-F. Berret, Shear-Induced Transitions and Instabilities in Surfactant Wormlike Micelles, in: K. Dusek, J.F. Joanny (Eds.) Polymer Characterization: Rheology, Laser Interferometry, Electrooptics, Springer-Verlag, Berlin Heidelberg, 2010, pp. 1-71.
[10] R.G. Larson, *The Structure and Rheology of Complex Fluids*, Oxford University Press, New York, 1998.
[11] A. Nussinovitch, *Hydrocolloid Applications: Gum technology in the food and other industries* Springer Science+Business Media, Dordrecht, 1997.
[12] M.J. Dulfano, K. Adler, W. Philippoff, Sputum Viscoelasticity in Chronic Bronchitis, *Am. Rev. Respir. Dis.*, 104 (**1971**) 88-98.
[13] M. King, Is Cystic-Fibrosis Mucus Abnormal, *Ped. Res.*, 15 (**1981**) 120-122.
[14] E. Puchelle, J.M. Zahm, F. Aug, Viscoelasticity, Protein-Content and Ciliary Transport Rate of Sputum in Patients with Recurrent and Chronic-Bronchitis, *Biorheology*, 18 (**1981**) 659-666.
[15] A. Jeanneret-Grosjean, M. King, M.C. Michoud, H. Liote, R. Amyot, Sampling Technique and Rheology of Human Tracheo-Bronchial Mucus, *Am. Rev. Respir. Dis.*, 137 (**1988**) 707-710.
[16] P.L. Shah, S.F. Scott, R.A. Knight, C. Marriott, C. Ranasinha, M.E. Hodson, In Vivo Effects of Recombinant Human Dnase I on Sputum In Patients with Cystic Fibrosis, *Thorax*, 51 (**1996**) 119-125.
[17] N.N. Sanders, S.C. De Smedt, E. Van Rompaey, P. Simoens, F. De Baets, J. Demeester, Cystic Fibrosis Sputum - A Barrier to the Transport of Nanospheres, *Am. J. Respir. Crit. Care Med.*, 162 (**2000**) 1905-1911.
[18] M. Dawson, D. Wirtz, J. Hanes, Enhanced Viscoelasticity of Human Cystic Fibrotic Sputum Correlates with Increasing Microheterogeneity in Particle Transport, *Journal of Biological Chemistry*, 278 (**2003**) 50393-50401.

[19] G.J. Besseris, D.B. Yeates, Rotating Magnetic Particle Microrheometry in Biopolymer Fluid Dynamics: Mucus Microrheology, *J. Chem. Phys.*, 127 (**2007**) 105106.
[20] J.S. Suk, S.K. Lai, Y.-Y. Wang, L.M. Ensign, P.L. Zeitlin, M.P. Boyle, J. Hanes, The Penetration of Fresh Undiluted Sputum Expectorated by Cystic Fibrosis Patients by Non-Adhesive Polymer Nanoparticles, *Biomaterials*, 30 (**2009**) 2591-2597.
[21] J. Seagrave, H.H. Albrecht, D.B. Hill, D.F. Rogers, G. Solomon, Effects of Guaifenesin, N-Acetylcysteine, and Ambroxol on Muc5ac and Mucociliary Transport in Primary Differentiated Human Tracheal-Bronchial Cells, *Respir. Res.*, 13 (**2012**) 98.
[22] J. Kirch, A. Schneider, B. Abou, A. Hopf, U.F. Schaefer, M. Schneider, C. Schall, C. Wagner, C.-M. Lehr, Optical Tweezers Reveal Relationship between Microstructure and Nanoparticle Penetration of Pulmonary Mucus, *Proc. Natl. Acad. Sci.*, 109 (**2012**) 18355-18360.
[23] B.S. Schuster, J.S. Suk, G.F. Woodworth, J. Hanes, Nanoparticle Diffusion in Respiratory Mucus from Humans Without Lung Disease, *Biomaterials*, 34 (**2013**) 3439-3446.
[24] G. Tomaiuolo, G. Rusciano, S. Caserta, A. Carciati, V. Carnovale, P. Abete, A. Sasso, S. Guido, A New Method to Improve the Clinical Evaluation of Cystic Fibrosis Patients by Mucus Viscoelastic Properties, *PLoS One*, 9 (**2014**) e82297.
[25] E.S. Vasquez, J. Bowser, C. Swiderski, K.B. Walters, S. Kundu, Rheological characterization of mammalian lung mucus, *RSC Adv.*, 4 (**2014**) 34780-34783.
[26] D.B. Hill, P.A. Vasquez, J. Mellnik*, et al.*, A Biophysical Basis for Mucus Solids Concentration as a Candidate Biomarker for Airways Disease, *PLoS One*, 9 (**2014**) e87681.
[27] S. Yuan, M. Hollinger, M.E. Lachowicz-Scroggins*, et al.*, Oxidation Increases Mucin Polymer Cross-Links to Stiffen Airway Mucus Gels, *Science Translational Medicine*, 7 (**2015**) 276ra227.
[28] X. Murgia, P. Pawelzyk, U.F. Schaefer, C. Wagner, N. Willenbacher, C.-M. Lehr, Size-Limited Penetration of Nanoparticles into Porcine Respiratory Mucus after Aerosol Deposition, *Biomacromolecules*, 17 (**2016**) 1536-1542.
[29] S. Requena, O. Ponomarchuk, M. Castillo*, et al.*, Imaging Viscosity of Intragranular Mucin Matrix in Cystic Fibrosis Cells, *Sci. Rep.*, 7 (**2017**) 16761.
[30] J.T. Ma, C. Tang, L. Kang, J.A. Voynow, B.K. Rubin, Cystic Fibrosis Sputum Rheology Correlates With Both Acute and Longitudinal Changes in Lung Function, *Chest*, 154 (**2018**) 370-377.
[31] T. Radtke, L. Boni, P. Bohnacker, P. Fischer, C. Bendend, H. Dressel, The Many Ways Sputum Flows - Dealing with High Within-Subject Variability in Cystic Fibrosis Sputum Rheology, *Respiratory Physiology & Neurobiology*, 254 (**2018**) 36-39.
[32] M. Jory, K. Bellouma, C. Blanc*, et al.*, Mucus Microrheology Measured on Human Bronchial Epithelium Culture, *Frontiers in Physics*, 7 (**2019**) 19.
[33] J. Patarin, É. Ghiringhelli, G. Darsy*, et al.*, Rheological analysis of sputum from patients with chronic bronchial diseases, *Sci. Rep.*, 10 (**2020**) 15685.
[34] M. Griese, E.M. App, A. Derouix, A. Burkert, A. Schams, Recombinant Human Dnase (Rhdnase) Influences Phospholipid Composition, Surface Activity, Rheology and Consecutively Clearance Indices of Cystic Fibrosis Sputum, *Pulmonary Pharmacology & Therapeutics*, 10 (**1997**) 21-27.
[35] D.J. Serisier, M.P. Carroll, J.K. Shute, S.A. Young, Macrorheology of cystic fibrosis, chronic obstructive pulmonary disease & normal sputum, *Respir. Res.*, 10 (**2009**) 63.